Optical Properties of ZnS Quantum Dots: Applications in Solar cells and Biomedicine

Rahul Singh [1,*] 🆔 , **Ragini Raj Singh** [1,*] 🆔

[1]   Department of Physics and Materials Science, Jaypee University of Information Technology, Waknaghat, Solan, Himachal Pradesh, India, 173234;rahur5.96@gmail.com(R.S.);raginirajsingh@gmail.com (R.R.S.);

*   Correspondence:rahur5.96@gmail.com(R.S.);raginirajsingh@gmail.com(R.R.S.);

Abstract: Optoelectronics and optical filter applications require wide bandgap semiconductors as photo-anode and surface passivation layers in sensitized solar cells and biomedical and biosensors fields such as optical filters [1–4]. Selecting suitable wide bandgap semiconductors increases the valuable implementation of desired devices. However, bulk semiconductors harvest only a particular spectrum, QDs help in harvesting large radiation spectra because of the tunable bandgap. Also, aqueous-based methods are eco-friendly, economical, biocompatible, and non-toxic. Therefore, in this study, ZnS quantum dots (QDs) were synthesized at 9.5 pH and $70^{\circ}C$ temperature using an aqueous-based chemical route method. A comparative study was presented using hydrazine hydrate and ammonium chloride as reducing agents for Zinc precursor and 3-mercaptopropionic acid (MPA) as capping agents. Confinement was achieved in ZnS using MPA as a stabilizer. Optical properties were studied using a photoluminescence (PL) spectrophotometer where photoluminescence (PL) shows emission behavior and photoluminescence excitation (PLE) shows excitation behavior of ZnS. Emission peaks were observed at 386 nm in as-prepared ZnS NPs and at 316 nm in confined QDs. Sharp band edge luminescence and the possibility to confine ZnS NPs show its eligibility in optoelectronics and optical filters in biological applications.

Keywords: wide band gap semiconductors; quantum dots; Bohr exciton radius; quantum dot sensitized solar cell (QDSSC); zinc sulfide.

1. Introduction

Wide bandgap (WBG) semiconductors (III-V, II-VI, and IV group materials) are the extensive research materials for major application fields like optical filters [1], solar cells [2,5–8], UV sensors [4], light-emitting diodes (LED) [9,10] along with biomedical applications such as optical imaging [3,11], bioelectronics [12] and as antibacterial agents [13]. The field of application depends on these materials' size, properties, and behavior in different conditions and at different parameters. The nanomaterial properties (optical, electrical, etc.) vary drastically when the size of the particle approaches exciton Bohr diameter following quantum confinement effect. Such nanomaterials are then called quantum dots (QDs) [14]. As compared with bulk materials, these QDs have properties like tunable bandgap, multiple exciton generation (MEG), high absorption coefficient and singlet-to-triplet exciton conversion, size-dependent PL, narrow band-edge luminescence [15,16], which make them unique (in optical, biomedical, etc.) to be used in above-mentioned applications[17,18]. Thus, choosing a suitable WBG QD material for a particular application helps harvest all valuable characteristics.

Among all WBG semiconductors, zinc sulfide (ZnS) is a promising candidate for optical applications due to its unique properties. Being an II-VI compound, it has a wide direct bandgap, 2.5 nm exciton Bohr radius, exciton binding energy of 39 meV along with economic, eco-friendly, and chemical stability status [19–21], which is suitable for optical applications since the optical property of a material depends on the bandgap which can be tuned by varying the particle size near to the exciton Bohr radius. Also, the ratio of reducing agent to precursor salt decides the reaction mechanism of the solution, which alters the NPs properties [22]. Till now, researchers used various methods along with different precursors, complexing agents, and capping agents to synthesize ZnS QDs. Li *et al*. have reported an aqueous method using 3-mercaptopropionic acid (MPA) and 3-mercaptopropyl (MPS) for ZnS QDs and resulted in MPS-replaced ZnS QDs to give better chemical stability and excellent PL intensity with high quantum yield (about 75%) when compared with MPA/ZnS QDs and MPS/ZnS QDs [23]. Mohammed and Salah used a chemical method to synthesize ZnS QDs using zinc chloride and sodium sulfide for hybrid QDs-LED devices using different cathode materials and found that lithium florid was better in the light enhancement process as compared to aluminum [24]. Karimi *et al*. studied the effect of capping agents (2-mercaptoethanol and 1-cysteine) using a water-based precipitation method to synthesize ZnS QDs and reported the high photocatalytic and chemically stable QDs [25]. Also, the last two years' research on ZnS QDs shows its contribution as photocatalyst[26–28], optical sensors[29,30], LEDs[31–34], and also in biological application[35–37].

To the best of our knowledge, no studies have been done on zinc chloride using hydrazine hydrate and ammonium chloride collectively. Therefore, in this paper, we have reported a cost-effective method (aqueous-based chemical route) to synthesize ZnS QDs using zinc and sulfur precursor, hydrazine hydrate, and ammonium chloride as reducing agents 3-mercaptopropionic acid (MPA) as a capping agent. Also, a comparative study has been done for hydrazine hydrate and ammonium chloride as separate reducing agents without capping agent and another sample of hydrazine hydrate with a capping agent to obtain better results for ZnS QDs.

2. Materials and Methods

2.1. Materials.

Zinc Chloride dry ≥95% ($ZnCl_2$), Hydrazine Hydrate 80% (N_2H_4), Ammonium Chloride ≥99% (NH_4Cl), Ammonia solution 25% (NH_3), Thiourea ≥99% ($SC(NH_2)_2$), 3-Mercaptopropionic acid ≥99% (MPA), Double distilled water. All chemicals used were of analytical grade.

2.2. Synthesis method & characterization.

ZnS QDs were synthesized using a one-step aqueous-based chemical route method. The molar concentration of 0.0250:0.0285 M for zinc chloride and thiourea, respectively was taken for the synthesis. Solution pH was set at 9.5, and the reaction proceeded at 70°C. Firstly, 50 ml solution was prepared using zinc chloride salt and stirred well. The simultaneously reducing agent was added in solution for all samples: ammonium chloride in Sample-A, hydrazine hydrate in Sample-B, and Sample-C. Ammonia solution was then added to set the pH value at 9.5 for all three samples. At 70°C, thiourea was added as a precursor in all samples, and MPA was added as a capping agent only in Sample-C. Sample-A and Sample-B were prepared

without a capping agent. Then, the reaction proceeded for 3 hours. The obtained nanoparticles were then washed by centrifugation, and samples were collected. As- prepared samples were characterized by photoluminescence spectrophotometer (Perkin Elmer LS-55) for PL and PLE measurements.

3. Results and Discussion

Characterization was done for optical properties (Photoluminescence and Photoluminescence excitation) using PL spectrophotometer at room temperature. This characterization gives detailed and precise information regarding the defects, surface traps present in the system and band edge luminescence, emission peaks, and excitation peaks of the prepared samples.

3.1. Photoluminescence (PL).

Figure 1-3 shows the PL spectra of as-synthesized ZnS nanoparticles. Peak positions, peak intensity values, and full width at half maxima (FWHM) were determined for all the samples using deconvolution of PL spectra and presented in Table 1-3. Figure 1(a) represents PL spectra of Sample-A ZnS nanoparticles synthesized using zinc chloride and thiourea as precursors and ammonium chloride as reducing agents. Five emission peaks were observed at different positions. Positions of emission peaks were recorded at 386 nm, 426 nm, 444 nm, 489 nm, and 540 nm. The emission peak corresponding to 386 nm was observed for band edge luminescence, and all other peaks represent zinc and sulfur defect states. Deconvolution was done to interpret the correct peak position and FWHM, shown in Figures 1(b) & 1(c). Figure 1(b) was a cumulative fit for the observed PL spectra but unfit for peak intensity values (Peak 2, Peak 3, and Peak 4). Thus, Figure 1(b) was modified by not disturbing the emission peak values, and the correct peak intensity value was calculated from Figure 1(c). Respective data is presented in Table 1.

Similarly, Figure 2(a) represents Sample-B ZnS NPs prepared using hydrazine hydrate as a complexing agent. Emissions peaks were observed at 426 nm, 447 nm, 489 nm, and 534 nm, along with the band edge emission at 392 nm. Figures 2(b) and 2(c) present deconvoluted graphs for correct peak positions using cumulative fit PL spectra and correct peak intensity value and respective FWHM, respectively. Corresponding data is presented in Table 2.

Emission peaks observed in both figures (Figure 1 and Figure 2) at 426 nm remain fixed, while the peak at 444 nm has a redshift to 447 nm. These defects are accredited to the defects for sulfur vacancies and interstitial zinc. Also, peak fixed at 489 nm was accredited to zinc vacancy. The peak at 540 nm is blue-shifted to 534 nm and is accredited to the recombination of electron-hole from energy levels of sulfur vacancy to zinc vacancy, respectively [11,38,39].

We have also compared the PL spectra of Sample-A and Sample-B and observed that the intensity of band edge luminescence and defects emission peaks of Sample-B get enhanced. The surface defects in Sample-B get reduced. The surface defects reduction resulted from hydrazine hydrate as a reducing agent. So we have used hydrazine hydrate to synthesize Sample-C, and due to the quantum confinement effect, surface area and defects get enhanced.
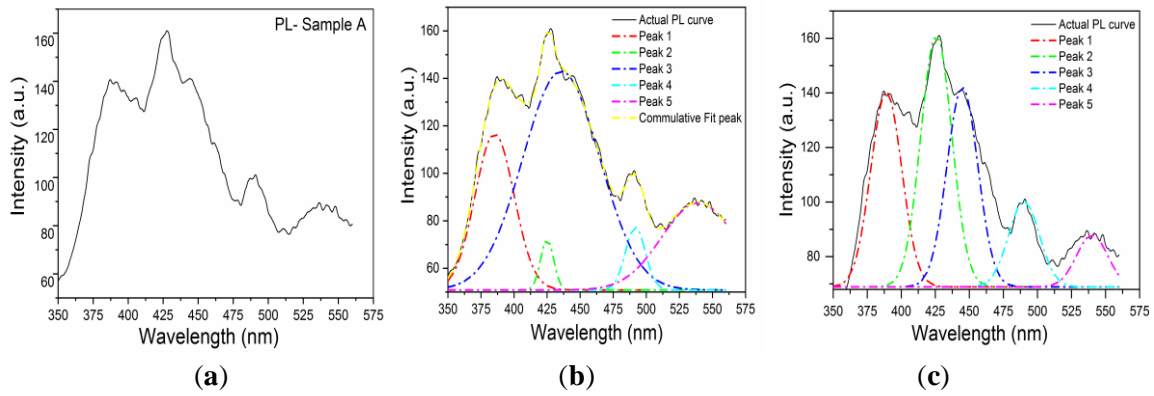
Figure 1. Sample-A:(**a**) PL spectra curve; (**b**) Deconvulated Graph for cumulative fit; (**c**) Deconvulated graph for measurement of actual peak intensity values.

Table 1. Peak position, peak intensity, and FWHM of Sample-A.

	Peak 1	Peak 2	Peak 3	Peak 4	Peak 5
Peak positions (nm)	386	426	444	489	540
Peak intensity (a.u.)	71.15	91.61	72.91	31.47	19.05
FWHM value	26.34	25.09	27.19	27.14	27.15
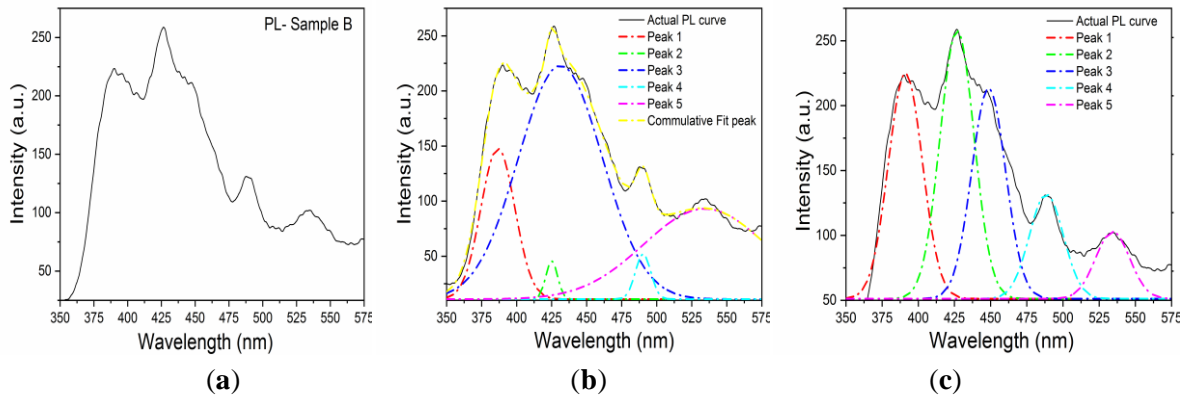
Figure 2. Sample-B:(**a**)PL spectra curve; (**b**) Deconvulated Graph for cumulative fit; (**c**) Deconvulated graph for measurement of actual peak intensity values.

Table 2. Peak position, peak intensity, and FWHM of Sample-B.

	Peak 1	Peak 2	Peak 3	Peak 4	Peak 5
Peak positions (nm)	392	426	447	489	534
Peak Intensity (a.u.)	173.32	206.80	161.41	80.08	51.07
FWHM value	27.17	27.95	27.56	27.58	28.64

(**a**)(**b**)(**c**)
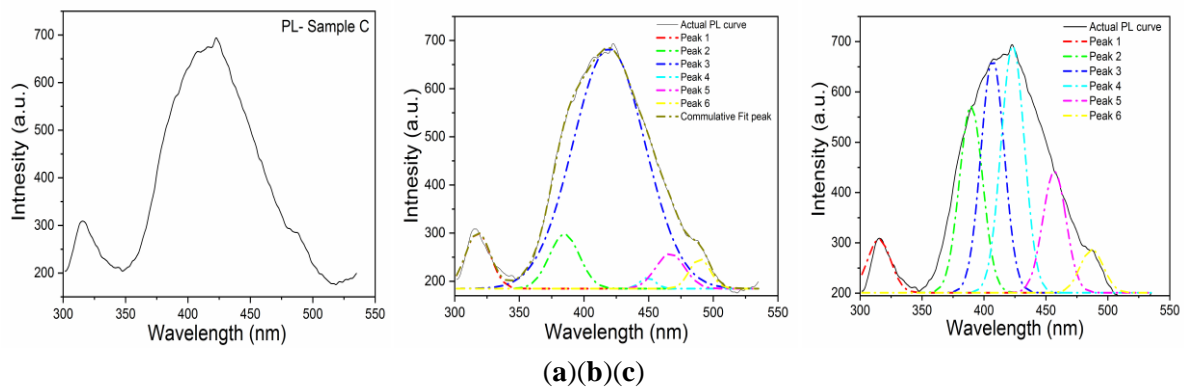
Figure 3. Sample-C: (**a**) PL spectra curve; (**b**) Deconvulated Graph for cumulative fit; (**c**) Deconvulated graph for measurement of actual peak intensity values.

Figure 3(a) represents the Sample-C ZnS QDs synthesized using hydrazine hydrate as reducing agent and MPA as capping agent. The band-edge emission peak was recorded at 316

nm along with the broad emission spectra from 346 nm to 480 nm containing multiple surface defect peaks and a small peak at 487 nm. Figures 3(b) and 3(c) represent deconvolution of the actual PL curve. Along with this, peak parameters are listed in Table 3.

Table 3. Peak position, peak intensity, and FWHM of Sample-C.

	Peak 1	Peak 2	Peak 3	Peak 4	Peak 5	Peak 6
Peak positions (nm)	316	390	407	423	457	487
Peak Intensity (a.u.)	114.26	368.66	462.80	489.30	239.99	84.96
FWHM value	21.43	23.07	21.84	22.24	22.96	20.13

The blue shift is observed here from 392 nm to 316 nm when the system was capped with MPA exhibiting quantum confinement. Also, an increase in the emission peak intensity and broadened emission spectrum for interstitial and vacancy defects represented an increase in surface-to-volume ratio when the confinement was achieved.

3.2 Photoluminescence excitation (PLE).

PLE spectra of all the samples for ZnS were presented in Figures 4-6. Figure 4 and Figure 5 represent PLE spectra of Sample-A and Sample-B of ZnS NPs, respectively. The excitation peak observed at 384 nm in Figure 4 corresponds to Sample-A's band edge emission peak at 386 nm. Similarly, Figure 5 excitation peak at 386 nm corresponds to the band edge emission observed at 392 nm in PL of Sample-B. Excitation near the band edge luminescence authenticates the observed values to be absorption peak values. Excitation peaks observed at 410 nm and 455 nm correspond to the defects observed between 400-450 nm and 489 nm, respectively, in PL spectra.
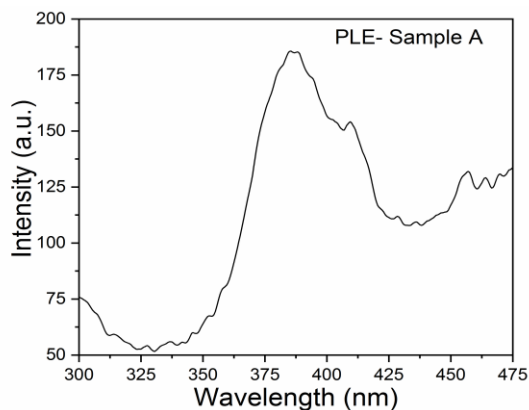
Figure 4. PLE spectra of Sample-A.　　　　**Figure 5.** PLE spectra of Sample-B.
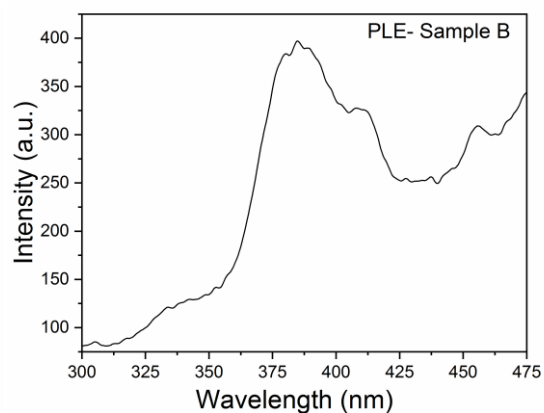
Figure 6 contains the information of PLE spectra of Sample-C. Figure 6(a) represents the recorded excitation from 200 nm up to 350 nm. Figure 6(b) represents the recorded excitation from 300 nm to 500 nm, thus giving whole excitation spectra from 250 nm up to 500nm. Excitation peaks observed in Figure 6(a) show the surface states and absorption peaks of ZnS QDs, while Figure 6(b) shows the absorption peak of ZnS QDs along with excitation peaks of surface defects. Both figures show an absorption peak at 305 nm for ZnS QD (band gap value of 4.05 eV). Along with this, excitation peaks at 377 nm and 412 nm were observed for surface defects.
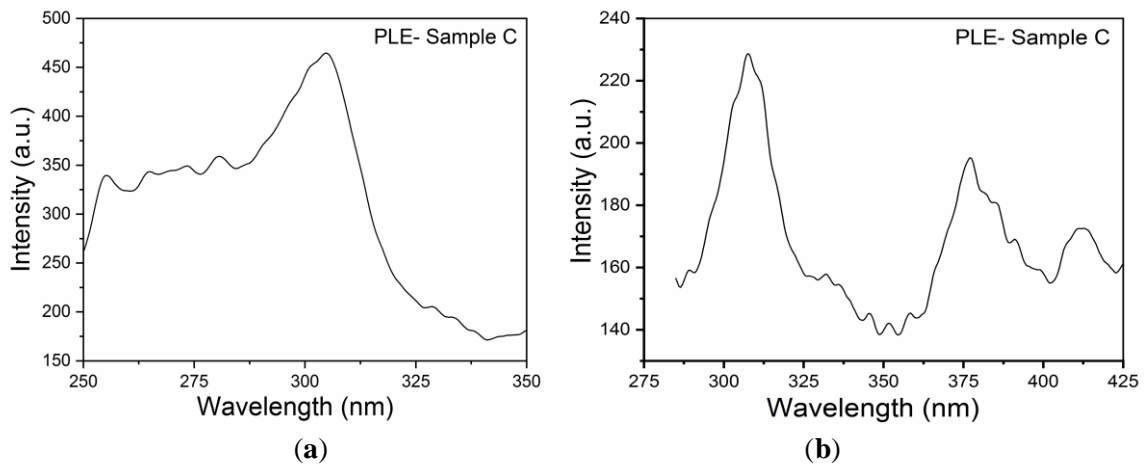
Figure 6. PLE of Sample-C from: (a) 200 nm to 350 nm; (b) 250 nm to 500 nm.

ZnS QD size was calculated using the Brus equation:

$$E_{g\ (QD)} = E_{g\ (bulk)} + \frac{h^2}{8R^2}\left(\frac{1}{m_{e*}} + \frac{1}{m_{h*}}\right) - \frac{1.786\ e^2}{4\pi\varepsilon_o\varepsilon_r R^2} \qquad (1)$$

where $E_{g\ (QD)}$ = band gap energy of QD material, $E_{g\ (bulk)}$ = band gap of bulk material, R = radius of quantum dot, h = Planck's constant, m_e* = effective mass of excited electron, m_h* = effective mass of excited hole, e = electronic charge, ε_o = vacuum permittivity, ε_r = relative permittivity.

The first term on the right side of equation (1) represents the bandgap of bulk material, the second term represents the addition of energy due to quantum confinement, and the third term represents the Coulombic interaction term between excitons which can be neglected because of R^{-2} and permittivity dependency. For ZnS material, bulk band gap value is 3.6 eV, m_e* = 0.34 m_o and m_h* = 0.23 m_o where m_o is the rest mass of electron [40]. ZnS QD radius was calculated and found to be 2.47 nm which is less than its exciton Bohr radius (2.5 nm), representing strong quantum confinement. For the other two samples (Sample-A and Sample-B), the Brus equation cannot be applied as these samples are not showing a quantum confinement effect.

4. Conclusions

This paper studied comparative optical properties (photoluminescence and photoluminescence excitation) for ZnS NPs using ammonium chloride and hydrazine hydrate as reducing agents in zinc chloride and thiourea as precursors. Emission peaks were observed at 386 nm and 392 nm, along with excitation peaks at 384 nm and 386 nm for ammonium chloride and hydrazine hydrate, respectively. Also, defects emission peaks were observed at 426 nm, 444 nm, 489 nm, and 540 nm for Sample-A, while for Sample-B, peaks were observed at 426 nm, 447 nm, 489 nm, and 534 nm. It was observed from PL spectra that different reducing agent affects the bandgap emission. Hydrazine hydrate enhances the emission peak intensity and reduces the surface traps.

Further, ZnS nanoparticles were capped using 3-mercaptopropionic acid (MPA), showing a strong quantum confinement effect. The emission peak was blue-shifted from 392 nm to 316 nm, and the absorption peak was blue-shifted from 386 nm to 305 nm. The bandgap value of ZnS QD was 4.05 eV, and QD size was found to be 4.94 nm using the Brus equation, which is less than the exciton Bohr diameter of ZnS (5.0 nm). Such wide bandgap material can be used in solar cells for surface passivation, for LEDs using band edge and fixed surface defects luminescence, optical imaging, and UV filters in biomedical applications.

Funding

Acknowledgments

Conflicts of Interest

The authors declare no conflict of interest.

References

1. Koç, K.; Tepehan, F.Z.; Tepehan, G.G. Preparation and Characterization of Self-Assembled Thin Film of MPS-Capped ZnS Quantum Dots for Optical Applications. *J.Nanomater.* **2012**, *2012*, e571315,https://doi.org/10.1155/2012/571315.

2. Mehrabian, M.; Mirabbaszadeh, K.; Afarideh, H. Solid-state ZnS quantum dot-sensitized solar cell fabricated by the Dip-SILAR technique. *Phys Scr.* **2014**, *89*, 085801,https://doi.org/10.1088/0031-8949/89/8/085801.

3. Deng, D.; Qu, L.; Gu, Y. Near-infrared broadly emissive AgInSe2/ZnS quantum dots for biomedical optical imaging. *J Mater Chem C.* **2014**, *2*, 7077–7085,https://doi.org/10.1039/C4TC01147C.

4. Premkumar, S.; Nataraj, D.; Bharathi, G.; Ramya, S.; Thangadurai, T.D. Highly Responsive Ultraviolet Sensor Based on ZnS Quantum Dot Solid with Enhanced Photocurrent. *Sci Rep.* **2019**, *9*, 18704,https://doi.org/10.1038/s41598-019-55097-8.

5. Ramya, M.; Nideep, T.K.; Nampoori, V.P.N.; Kailasnath, M. The impact of ZnO nanoparticle size on the performance of photoanodes in DSSC and QDSSC: a comparative study. *J Mater Sci: Mater Electron* **2021**, *32*, 3167–3179,https://doi.org/10.1007/s10854-020-05065-0.

6. Dutta, M.; Sarkar, S.; Ghosh, T.; Basak, D. ZnO/Graphene Quantum Dot Solid-State Solar Cell. *J Phys Chem C.* **2012**, *116*, 20127–20131,https://doi.org/10.1021/jp302992k.

7. Li, Z.; Yu, L.; Wang, H.; Yang, H.; Ma, H. TiO2 Passivation Layer on ZnO Hollow Microspheres for Quantum Dots Sensitized Solar Cells with Improved Light Harvesting and Electron Collection. *Nanomaterials* **2020**, *10*, 631,https://doi.org/10.3390/nano10040631.

8. Li, P.; Guo, L.; Chen, S.; Luo, G.; Zhu, S.; Wang, Y.; Song, L.; He, T. Facile modulation of different vacancies in ZnS nanoplates for efficient solar fuel production. *J Mater Chem A.***2021**, *9*, 7977–7990. https://doi.org/10.1039/D0TA12400A.

9. Wei, J.; Li, F.; Chang, C.; Zhang, Q. Synthesis of emission tunable AgInS2/ZnS quantum dots and application for light emitting diodes. *J. Phys. Commun.* **2020**, *4*, 045016,https://doi.org/10.1088/2399-6528/ab885a.

10. Xin, M.; Liao, L-M.; Han, F. Optical properties of ZnS: Ce nanocrystals prepared by hydrothermal method. *J. Lumin.***2021**, *238*, 118074,https://doi.org/10.1016/j.jlumin.2021.118074.

11. Kumari, A.; Thakur, N.; Vashishtt, J.; Singh, R.R. Structural, luminescent and antimicrobial properties of ZnS and CdSe/ZnS quantum dot structures originated by precursors. *Spectrochimica Acta Part A: Molecular and Biomolecular Spectroscopy* **2020**, *229*, 117962,https://doi.org/10.1016/j.saa.2019.117962.

12. Nguyen, N-K.; Nguyen, T.; Nguyen, T-K.; Yadav, S.; Dinh, T.; Masud, M.K.; Singha, P.; Do, T.N.; Barton, M.J.; Ta, H.T.; Kashaninejad, N.; Ooi, C.H.; Nguyen, N-T.; Phan, H-P. Wide-Band-Gap Semiconductors for Biointegrated Electronics: Recent Advances and Future Directions. *ACS Appl. Electron. Mater.* **2021**, *3*, 1959–1981,https://doi.org/10.1021/acsaelm.0c01122.

13. Baruah, J.M.; Kalita, S.; Narayan, J. Green chemistry synthesis of biocompatible ZnS quantum dots (QDs): their application as potential thin films and antibacterial agent. *Int Nano Lett.* **2019**, *9*, 149–159,https://doi.org/10.1007/s40089-019-0270-x.

14. Ramalingam, G.; Kathirgamanathan, P.; Ravi, G.; Elangovan, T.; Kumar, B.A.; Manivannan, N.; Kasinathan, K. Quantum Confinement Effect of 2D Nanomaterials. Quantum Dots - Fundamental and Applications; Divsar, F.; IntechOpen Limited: London, United Kingdom, **2020**; 70534,https://doi.org/10.5772/intechopen.90140.

15. Cassidy, J.; Zamkov, M. Nanoshell quantum dots: Quantum confinement beyond the exciton Bohr radius. *J Chem Phys.* **2020**, *152*, 110902,https://doi.org/10.1063/1.5126423.

16. Zaini, M.S.; Ying Chyi Liew, J.; Alang Ahmad, S.A.; Mohmad, A.R.; Kamarudin, M.A. Quantum Confinement Effect and Photoenhancement of Photoluminescence of PbS and PbS/MnS Quantum Dots. *Applied Sciences* **2020**, *10*, 6282,https://doi.org/10.3390/app10186282.

17. Liu, D.; Chen, L.; Chen, W.; Qin, M.; Wei, S. Enhanced visible-light photocatalytic activity of perylene diimide (PDI) supramolecular nanorods with Pt QDs deposited in situ. *Dalton Trans.* **2021**, *50*, 4008–4016,https://doi.org/10.1039/D0DT04356G.

18. Long, Z.; Tong, X.; Liu, C.; Channa, A.I.; Wang, R.; Li, X.; Lin, F.; Vomiero, A.; Wang, Z.M. Near-infrared, eco-friendly ZnAgInSe quantum dots-sensitized graphene oxide-TiO2 hybrid photoanode for high performance photoelectrochemical hydrogen generation. *Chem. Eng. J.* **2021**, *426*, 131298,https://doi.org/10.1016/j.cej.2021.131298.

19. D'Amico, P.; Calzolari, A.; Ruini, A.; Catellani, A. New energy with ZnS: novel applications for a standard transparent compound. *Sci Rep.* **2017**, *7*, 16805,https://doi.org/10.1038/s41598-017-17156-w.

20. Kumbhojkar, N.; Nikesh, V.V.; Kshirsagar, A.; Mahamuni, S. Photophysical properties of ZnS nanoclusters. *J. Appl. Phys.* **2000**, *88*, 6260–6264,https://doi.org/10.1063/1.1321027.

21. Komal; Shikha, P.; Kang, T.S. Facile and green one pot synthesis of zinc sulphide quantum dots employing zinc-based ionic liquids and their photocatalytic activity. *New J. Chem.* **2017**, *41*, 7407–7416,https://doi.org/10.1039/C7NJ01373F.

22. Sengupta, S.; Aggarwal, R.; Golan, Y. The effect of complexing agents in chemical solution deposition of metal chalcogenide thin films. *Mater Chem Front.* **2021**, *5*, 2035–2050,https://doi.org/10.1039/D0QM00931H.

23. Li, H.; Shih, W.Y.; Shih, W-H. Highly Photoluminescent and Stable Aqueous ZnS Quantum Dots. *Ind. Eng. Chem. Res.* **2010**, *49*, 578–582,https://doi.org/10.1021/ie901086d.

24. Mohammed, A.F.; Salah, W.R. Synthesis of ZnS Quantum Dots for QDs-LED hybrid device with different cathode materials. *J Phys: Conf Ser.* **2018,** *1032*, 012010,https://doi.org/10.1088/1742-6596/1032/1/012010.

25. Karimi, F.; Rajabi, H.R.; Kavoshi, L. Rapid sonochemical water-based synthesis of functionalized zinc sulfide quantum dots: Study of capping agent effect on photocatalytic activity. *Ultrasonics Sonochemistry* **2019**, *57*, 139–146,https://doi.org/10.1016/j.ultsonch.2019.05.019.

26. Juine, R.N.; Sahu, B.K.; Das, A. Recyclable ZnS QDs as an efficient photocatalyst for dye degradation under the UV and visible light. *New J. Chem.* **2021**, *45*, 5845–5854,https://doi.org/10.1039/D1NJ00588J.

27. Ca, N.X.; Vinh, N.D.; Bharti, S.; Tan, P.M.; Hien, N.T.; Hoa, V.X.; Peng, Y.; Do, P.V. Optical properties of Ce3+ and Tb3+ co-doped ZnS quantum dots. *Journal of Alloys and Compounds* **2021**, *883*, 160764,https://doi.org/10.1016/j.jallcom.2021.160764.

28. Sharma, K.; Raizada, P.; Hasija, V.; Singh, P.; Bajpai, A.; Nguyen, V-H.; . ZnS-based quantum dots as photocatalysts for water purification. *Journal of Water Process Engineering* **2021**, *43*, 102217,https://doi.org/10.1016/j.jwpe.2021.102217.

29. Díaz-Álvarez, M.; Martín-Esteban, A. Molecularly Imprinted Polymer-Quantum Dot Materials in Optical Sensors: An Overview of Their Synthesis and Applications. *Biosensors* **2021**, *11,*https://doi.org/10.3390/bios11030079.

30. Poornaprakash, B.; Chalapathi, U.; Kumar, M.; Vattikuti, S.V.P.; Rajitha, Beerelli.; Poojitha, P.T.; Park, Si-Hyun. Tailoring the optical and magnetic properties of ZnS nanoparticles via 3d and 4f elements co-doping. *Mater. Sci. Semicond. Process.* **2021**, *121*, 105395,https://doi.org/10.1016/j.mssp.2020.105395.

31. Li, H.; Jiang, X.; Wang, A.; Chu, X.; Du, Z. Simple Synthesis of CuInS2/ZnS Core/Shell Quantum Dots for White Light-Emitting Diodes. *Front. Chem.* **2020**, *8*, 669,https://doi.org/10.3389/fchem.2020.00669.

32. Zhang, W.; Ding, S.; Zhuang, W.; Wu, D.; Liu, P.; Qu, X.; Liu, H.; Yang, H.; Wu, Z.; Wang, K.; Sun, X.W. InP/ZnS/ZnS Core/Shell Blue Quantum Dots for Efficient Light-Emitting Diodes. *Adv. Funct. Mater.* **2020**, *30*, 2005303,https://doi.org/10.1002/adfm.202005303.

33. Xu, B.; Chen, H.; Zhang, T.; Long, Q.; Huang, L.; Li, D.; Zhang, Z.; Huang, Z.; Li, Q.; Jin, X. High quality quarternary-alloyed ZnCdSSe/ZnS quantum dots with single photoluminescence decay channel and high devise stability.*J. Lumin.* **2021**, *240*, 118463,https://doi.org/10.1016/j.jlumin.2021.118463.

34. Li, K.; Ye, Y.; Zhang, W.; Hu, Y.; Yang, Y.; Zhou, Y.; Liu, C. Modulation of the optical properties of ZnS QD-embedded glass through aluminum and manganese doping. *J Mater Chem C.* **2021**, *9*, 11261–11271,https://doi.org/10.1039/D1TC02285G.

35. An, J.; Huynh, K-H.; Ha, Y.; Jung, H.S.; Kim, H-M.; Kim, D-M.; Kim, J.; Pham, X-H.; Kim, D-E.; Ho, J-N.; Lee, S.; Lee, H-Y.; Jeong, D.H.; Jun, B-H. Surface Modification of a Stable CdSeZnS/ZnS Alloy Quantum Dot for Immunoassay. *J. Nanomater.* **2020**, *2020*, e4937049,https://doi.org/10.1155/2020/4937049.

36. Reshma, V.G.; Rajeev, K.S.; Manoj, K.; Mohanan, P.V. Water dispersible ZnSe/ZnS quantum dots: Assessment of cellular integration, toxicity and bio-distribution. *J. Photochem. Photobiol. B: Biol.* **2020**, *212*, 112019,https://doi.org/10.1016/j.jphotobiol.2020.112019.

37. Mostafa, M.; El Nady, J.; Ebrahim, S.M.; Elshaer, A.M. Synthesis, structural, and optical properties of Mn2+ doped ZnS quantum dots for biosensor application. *Opt. Mater.* **2021**,*112*, 110732,https://doi.org/10.1016/j.optmat.2020.110732.

38. Hu, P.; Liu, Y.; Fu, L.; Cao, L.; Zhu, D. Self-Assembled Growth of ZnS Nanobelt Networks. *J. Phys. Chem. B.* **2004**, *108*, 936–938,https://doi.org/10.1021/jp036743z.

39. Hou, L.; Gao, F. Phase and morphology controlled synthesis of high-quality ZnS nanocrystals. *Materials Letters* **2011**, *65*, 500–503,https://doi.org/10.1016/j.matlet.2010.10.061.

40. Chukwuocha, E.O.; Onyeaju, M.C.; Harry, T.S.T. Theoretical Studies on the Effect of Confinement on Quantum Dots Using the Brus Equation. *World J. Condens. Matter Phys.* **2012**, *2*, 96–100,https://doi.org/10.4236/wjcmp.2012.22017.